CHEMISTRY OF MATERIALS
Article

Chem. Mater. **2009,** *21,* 4685–4691 4685
DOI:10.1021/cm9018327

Highly Luminous Hollow Chloroapatite Phosphors Formed by a Template-Free Aerosol Route for Solid-State Lighting

Wei-Ning Wang, Yutaka Kaihatsu, Ferry Iskandar, and Kikuo Okuyama*

Department of Chemical Engineering, Graduate School of Engineering, Hiroshima University, 1-4-1 Kagamiyama, Higashi Hiroshima 739-8527, Japan

Received June 27, 2009. Revised Manuscript Received August 22, 2009

Highly luminous hollow chloroapatite blue phosphors were directly synthesized by an aerosol route. It is noteworthy that the hollow structures of the chloroapatite phosphors were achieved in a rapid manner (within several seconds) without using any templates, which offers tremendous advantages, such as saving time and energy, freedom from contamination, a lowering density, and a reduction of costs for both templates and raw materials. The as-prepared phosphors exhibited extremely high quantum efficiency (QE, as high as 100% under 365 nm excitation), showing great promise for white light-emitting diode (LED) application.

1. Introduction

White light-emitting diodes (LEDs), the so-called next generation of solid-state light (SSL), have attracted much attention because of their promise of energy savings and environmental protections.[1−3] These can be produced by several strategies, and an LED-plus-phosphor-based approach shows promise. To improve the SSL, a prominent quest has been the development of efficient phosphors, especially those that can illuminate under long ultraviolet (UV) excitation with high luminescence, small size, controllable morphology, and environmentally friendly characteristics.[1,4] White LEDs that are produced using these phosphors have high luminous efficacies and strong color stability.[1,5]

In general, phosphors used for the production of white LEDs should have a very high quantum efficiency (QE, $>95\%$), and both thermal and photochemical stability.[3,4] Also, the size, morphology, crystallinity, and stoichiometry of the phosphors must be controlled so that high luminous output can be achieved.[6] Nanophosphors may emerge as candidates,[7] because they demonstrate some interesting properties as a result of their small size.[8,9] There remains, however, a lack of compelling evidence of their actual application to white LEDs due to not only handling problems but the potential health risk and environmental impact, which heightens concern and may lead to strict regulations in the future.[10,11]

Therefore, development of an efficient phosphor with a slightly larger size that maintains some of the attractive features of nanoparticles is highly desirable, yet quite challenging. Besides the size, the particle morphology is another important factor we should pay attention to. The commercially available phosphors for white LEDs are usually irregular in shape, which gives rise to unnecessary loss due to random scattering on the particle surface upon illumination. A spheroid with smooth surface will be a good candidate. Furthermore, as we mentioned above, particles preserving nanoscale properties would be beneficial. In this sense, hollow and porous fine phosphors with spherical shape show promise because of their low density, high surface area, and hierarchical structures. They offer several advantages over nanophosphors, such as superior thermal stability, easy handling, and shape preservation.[12] For example, macroporous Y_2O_3:Eu phosphors were recently prepared and exhibited enhanced photoluminescence (PL).[13] Nevertheless, these phosphors are generally synthesized via a template method,[14] which requires post-treatment and may cause contamination, which can affect the PL property and subsequent applications.

*Corresponding author. E-mail: okuyama@hiroshima-u.ac.jp. Tel: 81-82-424-7716. Fax: +81-82-424-5494.

(1) Schubert, E. F.; Kim, J. K. *Science* **2005**, *308*, 1274.
(2) Bergh, A.; Craford, G.; Duggal, A.; Haitz, R. *Phys. Today* **2001**, *54*, 42.
(3) Phillips, J. M.; Coltrin, M. E.; Crawford, M. H.; Fischer, A. J.; Krames, M. R.; Mueller-Mach, R.; Mueller, G. O.; Ohno, Y.; Rohwer, L. E. S.; Simmons, J. A.; Tsao, J. Y. *Laser Photon. Rev.* **2007**, *1*, 307.
(4) Ogi, T.; Kaihatsu, Y.; Iskandar, F.; Wang, W.-N.; Okuyama, K. *Adv. Mater.* **2008**, *20*, 3235.
(5) Schubert, E. F. *Light-Emitting Diodes*; Cambridge University Press: New York, 2006.
(6) Wang, W.-N.; Widiyastuti, W.; Ogi, T.; Lenggoro, I. W.; Okuyama, K. *Chem. Mater.* **2007**, *19*, 1723.
(7) Colvin, V. L.; Schlamp, M. C.; Alivisatos, A. P. *Nature* **1994**, *370*, 354.
(8) Kompe, K.; Borchert, H.; Storz, J.; Lobo, A.; Adam, S.; Moller, T.; Haase, M. *Angew. Chem., Int. Ed.* **2003**, *42*, 5513.
(9) Takeshita, S.; Isobe, T.; Niikura, S. *J. Lumin.* **2008**, *128*, 1515.
(10) Colvin, V. L. *Nat. Biotechnol.* **2003**, *21*, 1166.
(11) Shimada, M.; Wang, W.-N.; Okuyama, K.; Myojo, T.; Oyabu, T.; Morimoto, Y.; Tanaka, I.; Endoh, S.; Uchida, K.; Ehara, K.; Sakurai, H.; Yamamoto, K.; Nakanishi, J. *Environ. Sci. Technol.* **2009**, *43*, 5529.
(12) Okuyama, K.; Abdullah, M.; Lenggoro, I. W.; Iskandar, F. *Adv. Powder Technol.* **2006**, *17*, 587.
(13) Widiyastuti, W.; Minami, T.; Wang, W.-N.; Iskandar, F.; Okuyama, K. *Jpn. J. Appl. Phys.* **2009**, *48*, 032001.
(14) Iskandar, F.; Mikrajuddin; Okuyama, K *Nano. Lett.* **2001**, *1*, 231.

Published on Web 09/11/2009

In addition, the precise control of stoichiometry of phosphor particles is of great importance, which affects the luminescent properties significantly. Because phosphors are generally composite materials, to maintain desired molar ratios of components during synthesis can be a difficult and complicated issue, especially for those having volatile components, such as chloroapatites.

In this work, we report the first direct synthesis of hollow chloroapatite blue phosphors with exceptionally high luminescence using a template-free aerosol route, i.e., a spray-pyrolysis (SP) method. Several unique aspects of this work merit highlighting upfront: (1) the chloroapatites are well-known lamp phosphors with low price and nontoxicity;[15] (2) the synthesis method is simple yet effective, with an extremely short processing time of several seconds;[16] (3) wonderful phosphor performance can be readily tailored by manipulating precursor properties and process parameters in a single step; and, (4) hollow structures were formed without using templates, which avoids contamination and reduces cost.

2. Experimental Section

Synthesis. Chloroapatite phosphors, $M_5(PO_4)_3Cl_x:Eu^{2+}$ (M = Ca, Sr, and Ba), were synthesized by the ultrasonic SP method using aqueous solutions of M nitrates ($M(NO_3)_2 \cdot 4H_2O$), M chlorides (MCl_2), europium nitrate ($Eu(NO_3)_3 \cdot 6H_2O$), phosphoric acid (H_3PO_4), and nitric acid (HNO_3), with a stoichiometric ratio of M:P:Cl:Eu = 1.00:0.58:1.74:0.01, as precursors. All chemicals were purchased from Kanto Chemical Co., Tokyo, Japan and used without further purification. H_2 (5 vol%) and N_2 (95 vol%) were used as the reductive and carrier gases, respectively. The solutions were atomized by means of an ultrasonic nebulizer operated at 1.7 MHz (NE-U17, Omron Healthcare Co., Ltd., Tokyo, Japan), and the mist was delivered by the gases into a tubular alumina reactor (1 m in length and 13 mm in inner diameter) maintained at predetermined temperatures, followed by heating for several seconds. The droplet size of the precursors was measured using a laser diffraction particle size system (Spraytec, Malvern Instruments Ltd., Worcestershire, UK), and the particles were collected in an electrostatic precipitator. The SP setup is schematically shown in the Supporting Information, Figure S1, and has been described in detail elsewhere.[6]

Characterization. The morphology and size of the phosphors were examined using field emission scanning electron microscopy (FESEM) (S-5000, Hitachi Corp., Tokyo, Japan). The mean diameters were determined by randomly sampling more than 500 particles from FESEM images. The inner structure was analyzed by transmission electron microscopy (TEM) (JEM-3000F, JEOL, Tokyo, Japan). Before TEM analysis, a small amount of the phosphor particles were first mixed with epoxy resin, then coated on a slide glass, followed by platinum ion sputtering before being cut into thin slices using a focused ion beam (FIB). The crystallinity was determined by X-ray diffraction (XRD) (RINT 2200 V, Rigaku Denki, Tokyo, Japan) using nickel-filtered Cu Kα radiation and selected area electron diffraction (SAED) coupled with the TEM. Elemental mapping and chemical composition were carried out using scanning transmission electron microscopy (STEM) equipped with energy-dispersive X-ray spectroscopy (EDS). PL spectra were recorded by means of a spectrofluorophotometer (RF-5300PC, Shimadzu Corp., Kyoto, Japan). The internal quantum efficiency was analyzed using an absolute PL quantum yield measurement system (C9920−02, Hamamatsu Photonics, Shizuoka, Japan) with a $BaSO_4$-coated integrating sphere. A Commission Internationale de I'Eclairage (CIE) 1931 XY chromaticity coordinate graph (XY diagram) was plotted for further analysis of the phosphors. All PL analyses were carried out under excitation of 365 nm at room temperature.

White LED Fabrication. UV LED chips (NSHU550B, Nichia Co., Tokyo, Japan) emitting a peak wavelength of 365 nm, were used in the fabrication of white LEDs. Prior to manufacturing, the phosphor particles (0.5 g), i.e., the chloroapatites together with commercial cerium-doped yttrium aluminum garnet (YAG:Ce), were first ultrasonically dispersed in ethanol (50 g) to form a homogeneous suspension, which was then blended with a polyvinylpyrrolidone (PVP) resin, with a weight ratio of 3:1, followed by beads-milling for 3 h to obtain a transparent phosphor-polymer suspension. Finally, a drop of the above suspension was deposited on the UV LED die, which was allowed to dry at room temperature for 6 h for solidification.

3. Results and Discussion

Effect of Synthesis Temperature. The chloroapatite phosphor particles were prepared via the SP method, which our group has spent a great deal of time to develop for various phosphors.[17−19] At the outset, we conducted a series of experiments to determine the optimal process parameters to be used in preparing calcium chloroapatite (abbreviated hereafter as Ca-apatite) phosphors. The effect of synthesis temperature, an important parameter in the SP process determining particle formation, was first investigated. As shown in the FESEM images, the Ca-apatite particles obtained at all temperatures had a similar morphology and size (Figure 1a). However, the corresponding digital photos displayed different emission colors. Their PL spectra in Figure 2 confirmed that in addition to the main blue emission peak at approximately 450 nm, there were also several other peaks in the orange and red regions. In particular, for preparations at higher temperatures, such as 1400 °C, the main emission peak is very weak, whereas the others are prominent. The color of the phosphors thus was a mixture of blue and others. The photos show that dark magenta and medium orchid were observed at 800 and 900 °C, respectively, which were considered to be caused by the slow reduction of H_2 with Eu^{3+}. Blue color appeared only at a certain temperature—1100 °C. Afterward, the color surprisingly changed to pale purple at 1200 °C and eventually red at 1400 °C, which seemed unreasonable and perplexing; the answer,

(15) Butler, K. H. *Fluorescent Lamp Phosphors*; Pennsylvania State University Press: University Park, PA, 1980.
(16) Okuyama, K.; Lenggoro, I. W. *Chem. Eng. Sci.* **2003**, *58*, 537.
(17) Kang, Y. C.; Park, S. B.; Lenggoro, I. W.; Okuyama, K. *J. Phys. Chem. Solids* **1999**, *60*, 379.
(18) Lenggoro, I. W.; Okuyama, K. Preparation of Fine Phosphor and Luminescent Micro/Nanoparticles Using Spray Pyrolysis. In *Handbook of Luminescence, Display Materials, and Devices − Inorganic Display Materials*; Nalwa, H. S., Rohwer, L. S., Eds.; American Scientific Publishers: Stevenson Ranch, CA, 2003; p 327.
(19) Wang, W.-N.; Iskandar, F.; Okuyama, K.; Shinomiya, Y. *Adv. Mater.* **2008**, *20*, 3422.

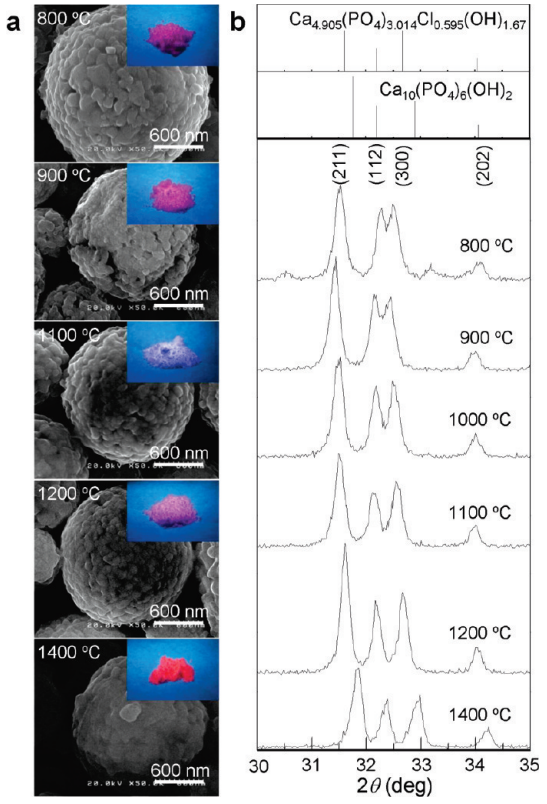

Figure 1. Calcium chloroapatite phosphor particles prepared at various synthesis temperatures. (a) FESEM images and their corresponding digital photos taken under 365 nm excitation. (b) XRD patterns. Representative Joint Committee on Powder Diffraction Standards (JCPDS) references for calcium chloroapatite and calcium hydroxyapatite are $Ca_{4.905}(PO_4)_{3.014}Cl_{0.595}(OH)_{1.67}$ (No. 700794) and $Ca_{10}(PO_4)_6(OH)_2$ (No. 740565), respectively. The phosphors were prepared at a precursor concentration of 0.10 M and a total gas flow rate of 5 L/min.

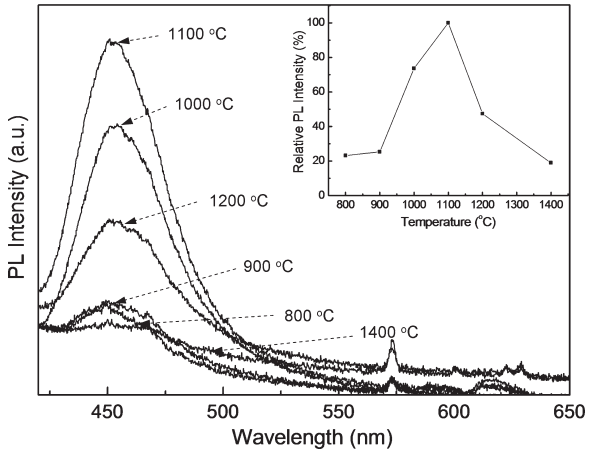

Figure 2. PL spectra of the chloroapatite phosphor particles at different synthesis temperatures. The inset shows the relative PL intensity at 450 nm as a function of temperature.

in essence, lay in their crystal phases. The corresponding XRD patterns in Figure 1b illustrate a constant right shift of (211), (112), and (300) planes with increasing temperature, indicating a crystal structure change from chloroapatite to hydroxyapatite because of the loss of chloride at

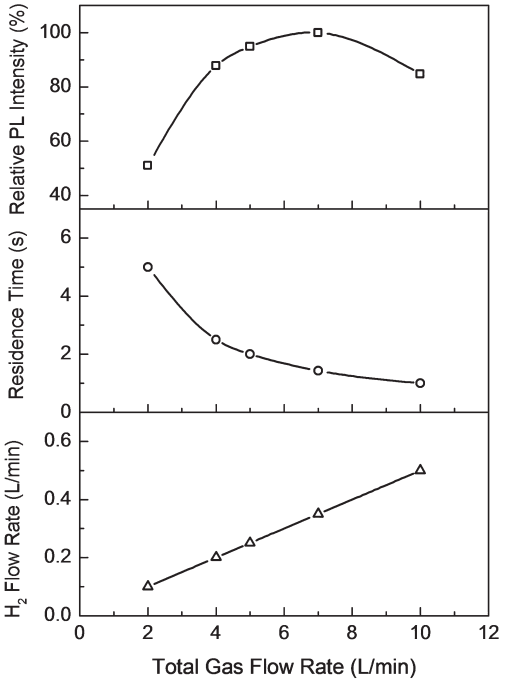

Figure 3. Relative PL intensity, residence time, as well as H_2 flow rate as a function of total gas flow rate. The synthesis temperature was fixed at 1100 °C.

high temperatures to form hydrogen chloride gases. Compared with chloroapatite, hydroxyapatite was not a preferable structure for Eu^{2+} emission.[19,20] Besides, the decreased residence time at elevated temperatures may have exacerbated the reduction reaction (see Figure S2 in the Supporting Information for details). The trade-off made 1100 °C the best temperature to use for the subsequent experiments.

Effect of Gas Flow Rate. In addition to the temperature effect, our experience in the SP process suggested that the gas flow rate played an important role as well. Figure 3 shows relative PL intensity, residence time, as well as H_2 flow rate as a function of total gas flow rate. From the figure, the relative PL intensity first increases gradually with increasing total gas flow rate. After reaching a maximum value at 7 L/min, however, it reverses, i.e., decreases with increasing total gas flow rate. The phenomenon is considered to be caused by the trade-off effects of residence time and H_2 flow rate induced by the variation of total gas flow rate. As shown in Figure S2 in the Supporting Information, the residence time is a function of the gas flow rate, the temperature, and the volume of the reactor. Keeping other parameters constant, a similar conclusion can be drawn from that of temperature, i.e., the higher the total gas flow rate, the shorter the residence time. Consequently, the reduction reaction will be hindered by increasing total gas flow rate. On the other hand, the H_2 flow rate increases with increasing total gas flow rate, which, however, can promote the reduction reaction. In addition to the above discussion, a total gas flow rate that is too high will cause an unstable heating flow inside the reactor. To keep the experiment under control, we selected 5 L/min

(20) Kottaisamy, M.; Jagannathan, R.; Jeyagopal, P.; Rao, R. P.; Narayanan, R. L. *J. Phys. D.* **1994**, *27*, 2210.

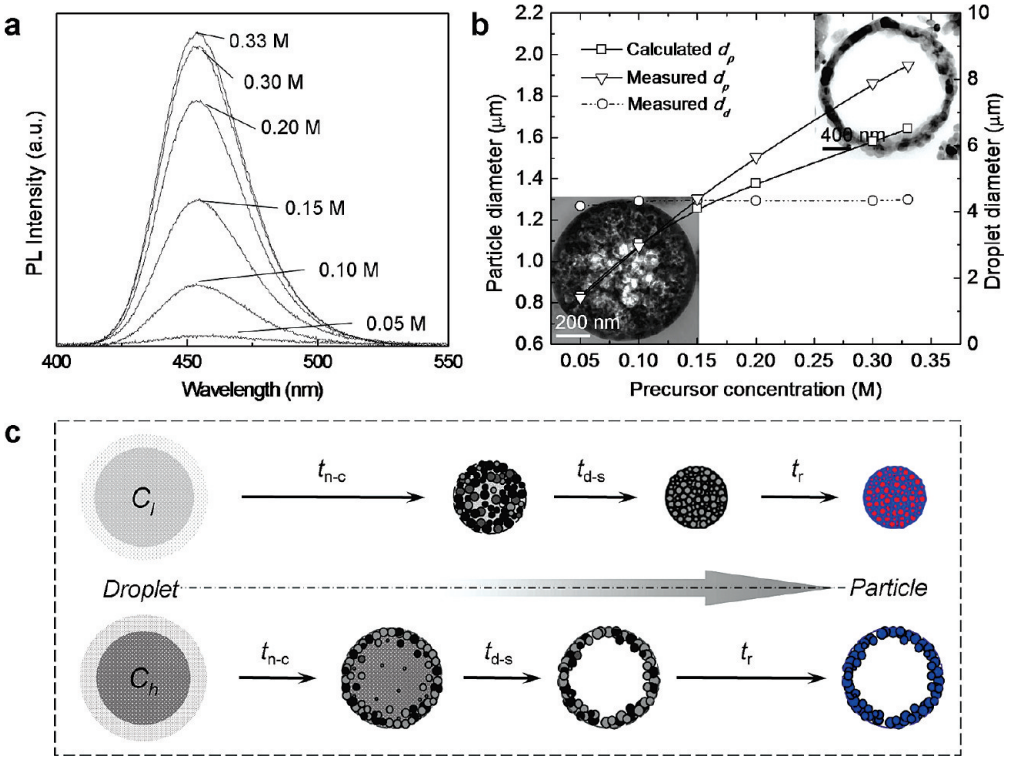

Figure 4. Influence of precursor concentration on PL properties and formation mechanisms of calcium chloroapatite phosphor particles. (a) PL emission spectra. (b) Correlations between precursor concentration and particle (d_p) as well as droplet diameters (d_d). The droplet sizes were found to be approximately constant at all concentrations. The insets are representative TEM images of the phosphors obtained at low (0.05 M, lower left) and high concentrations (0.33 M, upper right). c. Possible droplet-to-particle transformation mechanisms. C_l and C_h indicate low and high concentrations, respectively. $t_{n\text{-}c}$, $t_{d\text{-}s}$, and t_r represent characteristic times for nucleation-crystal growth, further drying-sintering, and reduction reaction, respectively. The total residence time is the sum of $t_{n\text{-}c}$, $t_{d\text{-}s}$, and t_r.

as the optimal gas flow rate for subsequent experiments.

Strategy to PL Enhancement. The process optimization previously discussed did have some effects on the PL enhancement. However, the as-prepared phosphors continued to have insufficient luminescence, making them unuseable for actual applications.

Improving the luminescence of phosphors formed via such a rapid process can be very tricky, because the reduction of Eu^{3+} to Eu^{2+} may be hindered. We attempted to substitute calcium with magnesium ions and to change the europium doping concentration, which worked and yielded a high QE of 80%.[19] Here we show another effective strategy, i.e., increasing precursor concentration.

The PL spectra in Figure 4a show that increasing the precursor concentration resulted in enhanced luminescence properties. The maximal PL intensity, with a QE as high as 92%, was obtained at 0.33 M. An even higher QE, i.e. 100%, was achieved at this concentration via Mg substitution, which again verified our previous report on Mg effect.[19] Detailed quantum efficiencies of apatite phosphors prepared at various conditions can be found in Table 1. The first reason for the PL enhancement may be attributed to the particle size effect.[6] Theoretically, the size of the particles formed in the SP process can be predicted based on the typical one-droplet-to-one-particle (ODOP) mechanism,[21] from which a more concentrated precursor produces larger particles, assuming the droplet size remains constant. However, the reality of the situation was more complex. Figure 4b shows a tendency for both calculated and measured particle diameters to increase with precursor concentration (see Figure S3 in the Supporting Information for details).[22] The measured particle diameters coincided well with the theoretical ones at low concentrations as evidenced by the corresponding TEM image (the lower left inset in Figure 4b); the deviation between them, however, became larger at higher concentrations, which indicated the formation of hollow particles.

The phenomenon can be explained by droplet-to-particle transformation mechanisms, as schematically shown in Figure 4c. In a typical SP process, droplets first undergo nucleation and crystallization, followed by further drying and sintering to form final particles.[23] A reduction reaction between H_2 and Eu^{3+} may happen simultaneously after the formation of solid particles. The residence time is assumed to be identical at the same synthesis temperature and gas flow rate. At a low concentration, the characteristic time for nucleation and crystallization, $t_{n\text{-}c}$, can be very long because of the slow supersaturation

(21) Wang, W.-N.; Widiyastuti, W.; Lenggoro, I. W.; Kim, T. O.; Okuyama, K. *J. Electrochem. Soc.* **2007**, *154*, J121.
(22) Wang, W.-N.; Purwanto, A.; Lenggoro, I. W.; Okuyama, K.; Chang, H.; Jang, H. D. *Ind. Eng. Chem. Res.* **2008**, *47*, 1650.
(23) Messing, G. L.; Zhang, S. C.; Jayanthi, G. V. *J. Am. Ceram. Soc.* **1993**, *76*, 2707.

Table 1. Quantum Efficiencies and Chromatic Properties of Chloroapatite Phosphors

		quantum efficiency	chromaticity coordinates		purity (%)	emission peak (nm)	peak count (cps)	tristimulus values		
			x	y				X	Y	Z
concentration effect ($Ca_{5.17}(PO_4)_3Cl_9$:Eu)	0.05 M	0.04	0.203	0.178	59.90	377.98	247.35	335.23	295.23	1023.56
	0.10 M	0.27	0.157	0.087	86.64	454.87	562.94	1431.29	792.62	6907.35
	0.15 M	0.43	0.150	0.066	91.96	455.62	1027.42	2486.20	1087.60	13010.77
	0.20 M	0.61	0.148	0.061	93.34	454.11	1678.09	3792.31	1566.69	20336.71
	0.30 M	0.76	0.145	0.056	94.68	453.36	2383.65	5139.37	2007.35	28431.43
	0.33 M	0.92	0.144	0.054	95.39	453.36	2565.05	5440.85	2046.73	30280.30
concentration effect ($Ca_{4.47}Mg_{0.7}(PO_4)_3Cl_9$:Eu)	0.10 M	0.35	0.151	0.068	91.19	454.87	796.58	1893.80	847.87	9761.42
	0.15 M	0.51	0.147	0.059	93.96	453.36	1249.59	2814.09	1121.79	15233.66
	0.20 M	0.82	0.145	0.055	95.07	453.36	1908.34	4157.58	1574.91	22963.11
	0.30 M	0.86	0.144	0.054	95.41	455.62	2196.73	4767.99	1770.44	26478.75
	0.33 M	1.00	0.142	0.053	96.10	455.87	2730.81	8224.65	9669.47	40142.18
composition effect	Sr-apatite	1.00	0.154	0.030	97.99	447.35	3213.40	6735.17	1305.22	35759.05
	Ba-apatite	0.99	0.156	0.044	94.60	434.56	3048.64	7134.15	2012.05	36532.69
commercial $BaMgAl_{10}O_{17}:Eu^{2+}$		1.00	0.156	0.044	94.71	434.56	3177.83	7407.77	2085.05	38048.55

rate, which occupies a large fraction of the total residence time. On the other hand, the time can be accelerated at higher concentrations,[23] saving more time for reduction. Therefore, an improved reduction reaction at higher concentrations is another important reason for PL enhancement.

The hollow particles formed at high concentrations, as shown in Figure 4c, were based on the typical surface precipitation theory.[23,24] The upper-right TEM image shown in Figure 4b confirms the formation of the hollow structures. It is noteworthy that the hollow structures of the chloroapatite phosphors were achieved in a rapid manner (within several seconds) without using templates, which offers tremendous advantages, such as saving time and energy, freedom from contamination, a lowering density, and a reduction of costs for both templates and raw materials.

In addition to the Ca-apatites, strontium chloroapatite (Sr-apatite) and barium chloroapatite (Ba-apatite) particles with similar hollow structures were also obtained (Figure 5). Close inspection of the images shows that the hollow particles actually consist of many primary nanocrystallites, as verified by the SAED patterns. These Sr- and Ba-apatite phosphors demonstrated great PL performance as well, having QE values of approximately 100% (see Table 1). Figure 6 shows the corresponding PL spectra. A blue shift of the PL peak wavelength is observed from Ca-apatite to Ba-apatite that can be explained by the compound's bond ionicity (P) theory, and is closely related to the g factor of Eu^{2+}, which is defined as $g = (1 - K^2)g(^8S_{7/2}) + K^2g(^6P_{7/2})$ according to Watanabe's theory,[25] where $K = 14^{1/2}\lambda(E_g - E_s)$ is the mixing component of the excited state ($^6P_{7/2}$) into the ground state ($^8S_{7/2}$), λ is the L−S coupling coefficient, and $E_g - E_s$ is the energy difference between the ground and the excited states. As the bond iconicity, P, increases, the g factor value increases, whereas the d−f emission of Eu^{2+} shifts to shorter wavelengths.[26]

Elemental Analysis. Phosphors made by other routes usually suffer from composition inhomogeneity owing to inefficient mixing and macroscopic reaction—such as in solid reaction routes—and difficulty in removing impurities, especially for those synthesized from liquid methods. By contrast, the SP method offers great controllability in composition distribution inside product particles because of the microscopic reactions in the fine droplets that serve as microreactors. As an example, the elemental mapping of the Ca-apatite in Figure 7 shows that all elements were distributed uniformly throughout the particle. In addition, the EDS results showed that the molar ratios of nearly all elements inside the particles were consistent with the stoichiometric ratio of M:P:Cl:Eu

(24) Kodas, T. T.; Hampden-Smith, M. J. *Aerosol Processing of Materials*; Wiley-VCH: New York, 1999.
(25) Watanabe, H. *Prog. Theor. Phys.* **1957**, *18*, 405.
(26) Chen, W. Luminescence, Storage Mechanisms, and Applications of X-Ray Storage Phosphors. In *Handbook of Luminescence, Display Materials, and Devices−Inorganic Display Materials*; Nalwa, H. S., Rohwer, L. S., Eds.; American Scientific Publishers: Stevenson Ranch, CA, 2003; p 1.

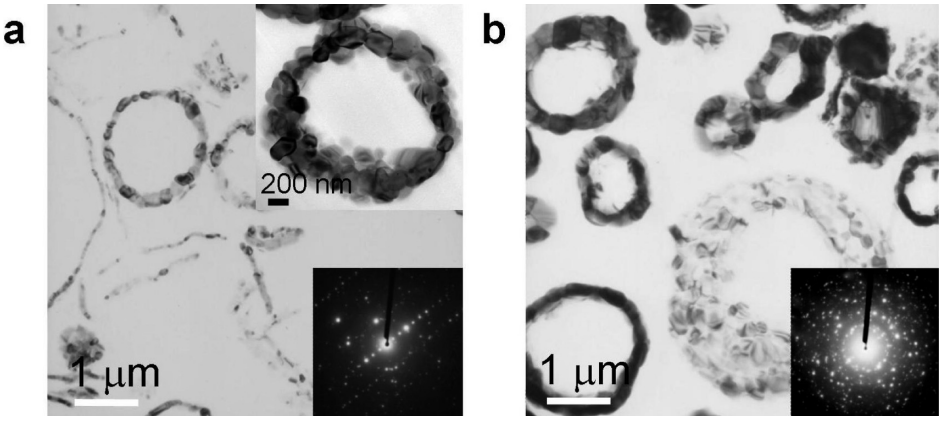

Figure 5. TEM images of strontium and barium chloroapatite phosphor particles. (a) Strontium chloroapatite. The insets are the magnified TEM image (upper right) and the SAED pattern. (b) Barium chloroapatite. The inset is the corresponding SAED pattern. The particles were prepared at 1100 °C with a total gas flow rate of 5 L/min, and precursor concentrations of 0.33 M for Sr-apatites and 0.20 M for Ba-apatites.

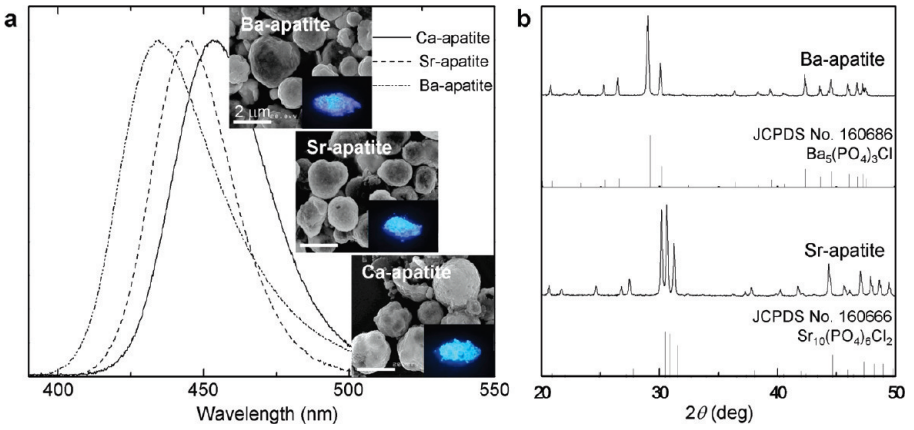

Figure 6. Representative PL spectra and XRD patterns of different chloroapatite phosphors. (a) Normalized PL spectra of Ca-, Sr-, and Ba-apatites. The insets show SEM images of three different chloroapatites and their corresponding digital photos. (b) XRD patterns of Sr- and Ba-apatites. Representative JCPDS references for strontium chloroapatite and barium chloroapatite are $Sr_{10}(PO_4)_6Cl_2$ (No. 160666) and $Ba_5(PO_4)_3Cl$ (No. 160686), respectively. The results show that both prepared phosphors agreed well with the references. The sharp peaks in the XRD patterns indicate their high crystallinity.

in the precursor solution. The drastic difference in the Cl ratio was caused by the loss of Cl, as stated before. The results of the elemental analysis of the Sr- and Ba-apatite phosphors can be found in the Supporting Information shown in Figure S4. No impurities were detected, which again proves the effectiveness and promise of the SP method, whereby simply manipulating the stoichiometric ratio of the precursors can control the composition of particles.

Chromatic Analysis and White LED Fabrication. The results from further PL analysis of the above phosphors are shown in the CIE chromaticity diagram (Figure 8). A blue color was detected for all samples. The chromaticity coordinates of the Ca-apatites deceased linearly with increasing precursor concentration indicating an increase in color purity and brightness. A brilliant pure blue color was achieved at 0.33 M with the coordinates of (0.144, 0.054). The Sr-apatite phosphor showed the lowest y coordinate (0.154, 0.030), whereas the Ba-apatite was an exact match of the commercial $BaMgAl_{10}O_{17}:Eu^{2+}$ (0.156, 0.044). Detailed chromaticity information can be found in Table 1.

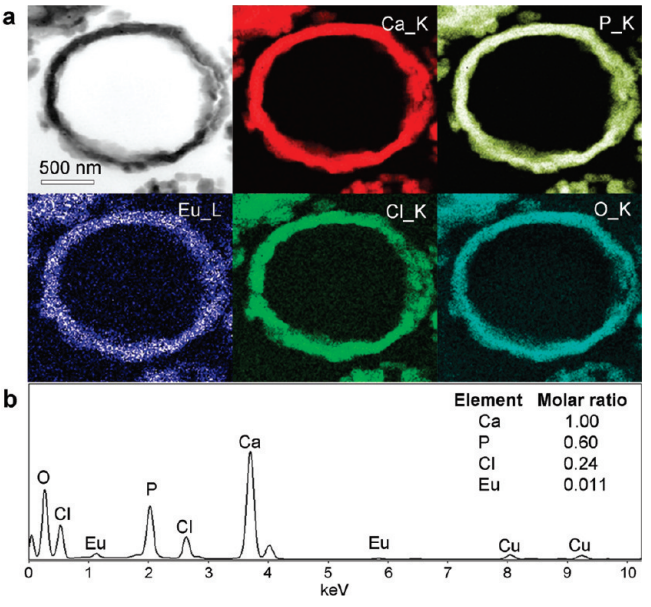

Figure 7. Elemental analysis of calcium chloroapatite particles. (a) STEM (upper left) and elemental mapping images. (b) EDS spectra. Elemental molar ratios are listed in the inset.

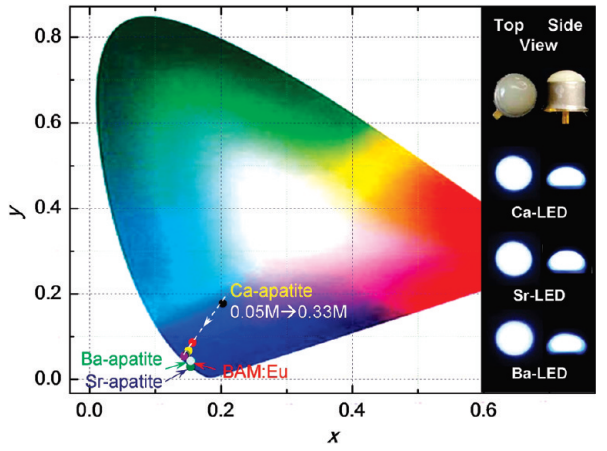

Figure 8. Chromaticity of chloroapatite phosphors and their application to white LEDs. (a) CIE chromaticity diagram. (b) Top and side views of white LEDs fabricated using Ca-, Sr-, and Ba-apatite with YAG:Ce phosphors, abbreviated as Ca-LED, Sr-LED, and Ba-LED, respectively.

To verify their application, we fabricated white LEDs by coating a transparent polymer resin containing the chloroapatite phosphors together with commercial YAG:Ce, on UV LED chips (see the Experimental Section for details). An intense white light was produced, as illustrated by the corresponding digital photos in Figure 8 (also see Figure S5 in the Supporting Information). White LEDs manufactured using the same procedure with UV chips in previous reports also exhibited remarkably high color rendering indices (CRIs) as well as quantum efficiencies, implying that replacement of the current mercury-based lamps is not a distant dream.[27,28]

4. Conclusions

The hollow chloroapatite phosphors were successfully synthesized using a one-step aerosol method. Strategies to improve the PL properties of the phosphors were investigated in detail. The phosphors demonstrated wonderful PL performance and hold great promise for SSL applications owing to their lightweight, low cost, and hierarchical structures. Work in this direction is in progress. We would be remiss in not mentioning that the results presented here show not only the beneficial properties processed by the chloroapatite phosphors, but also provide an example for the design of functional fine phosphors with tailored morphologies, such as hollow structures, in consideration of environmental and public health protection, which should be applicable to other phosphors in the foreseeable future.

Acknowledgment. We thank Shunsuke Kinouchi for his assistance in the spray pyrolysis experiments. We are grateful to Dr. Eishi Tanabe in Hiroshima Prefectural Institute of Industrial Science and Technology for his help with the TEM and EDS analyses. Grant-in-aids sponsored by the Japanese Ministry of Education, Culture, Sports, Science and Technology of (MEXT) and the Japan Society for the Promotion of Science (JSPS) are acknowledged (K.O.).

Supporting Information Available: Schematic diagram of the experimental setup; additional discussion on the temperature effect; SEM images of Ca-apatite particles at different concentrations; wlemental analysis of Sr- and Ba-apatites; white LEDs fabrication (PDF). This material is available free of charge via the Internet at http://pubs.acs.org.

(27) Morita, D.; Yamamoto, M.; Akaishi, K.; Matoba, K.; Yasutomo, K.; Kasai, Y.; Sano, M.; Nagahama, S.; Mukai, T. *Jpn. J. Appl. Phys.* **2004**, *43*, 5945.
(28) Radkov, E.; Setlur, A. A.; Brown, Z.; Reginelli, J. *Proc. SPIE* **2004**, *5530*, 260.